

Branching fractions for $P_{3/2}$ decays in Ba^+

Zhiqiang Zhang ¹, K. J. Arnold,^{1,2} S. R. Chanu,¹ R. Kaewuam,¹ M. S. Safronova,^{3,4} and M. D. Barrett ^{1,5,*}

¹Centre for Quantum Technologies, National University of Singapore, 3 Science Drive 2, 117543 Singapore

²Temasek Laboratories, National University of Singapore, 5A Engineering Drive 1, 117411 Singapore

³Department of Physics and Astronomy, University of Delaware, Newark, Delaware 19716, USA

⁴Joint Quantum Institute, National Institute of Standards and Technology and the University of Maryland, College Park, Maryland 20742, USA

⁵Department of Physics, National University of Singapore, 2 Science Drive 3, 117551 Singapore



(Received 5 March 2020; accepted 23 April 2020; published 24 June 2020)

Branching fractions for decays from the $P_{3/2}$ level in $^{138}\text{Ba}^+$ have been measured with a single laser-cooled ion. Decay probabilities to $S_{1/2}$, $D_{3/2}$, and $D_{5/2}$ are determined to be 0.741716(71), 0.028031(23), and 0.230253(61), respectively, which are an order-of-magnitude improvement over previous results. Our methodology only involves optical pumping and state detection, and is hence relatively free of systematic effects. Measurements are carried out in two different ways to check for consistency. Our analysis also includes a measurement of the $D_{5/2}$ lifetime, for which we obtain 30.14(40) s.

DOI: [10.1103/PhysRevA.101.062515](https://doi.org/10.1103/PhysRevA.101.062515)

I. INTRODUCTION

Singly ionized barium has been well studied over the years with a wide range of precision measurements [1–8] providing valuable benchmark comparisons with theory [9–14]. Such comparisons have been motivated in part by the proposed parity nonconservation measurement using the $S_{1/2}$ - $D_{3/2}$ transition in $^{137}\text{Ba}^+$ [15]. Recently, we have proposed that accurately measured properties of $^{138}\text{Ba}^+$ can be combined to provide an accurate model of the dynamic differential scalar polarizability $\Delta\alpha_0(\omega)$ for the $S_{1/2}$ - $D_{5/2}$ clock transition [16]. With such a model, ac Stark shifts of the clock transition could provide an *in situ* calibration of laser intensities and comparison of polarizabilities with another species. A limiting factor for the proposal was the accuracy of existing values for $P_{3/2}$ branching ratios. Moreover, recent measurements of $P_{1/2}$ branching fractions [17] indicated possible problems with existing $P_{3/2}$ values [8]. Consequently, we have remeasured these values with an order-of-magnitude improvement in their uncertainties.

Our measurements only involve optical pumping and state detection. Consequently, results are insensitive to laser intensity, frequency, and polarization changes provided they do not significantly affect optical pumping times and detection. Our implementation also allows the branching ratios to be determined in two different ways, which we do by way of a consistency check on our results.

II. EXPERIMENT OVERVIEW

The relevant level structure for Ba^+ is given in Fig. 1(a). Doppler cooling is provided by driving the transitions at 493 and 650 nm, with light scattered at 650 nm collected onto a

single-photon counting module for detection. The remaining three transitions at 455, 585, and 614 nm facilitate optical pumping as required. Throughout the paper, we refer to $S_{1/2}$ and $D_{3/2}$ states collectively as the bright state, and $D_{5/2}$ states as the dark state.

The experiments are carried out in a linear Paul trap with axial end caps as described in [18,19]. The laser configurations relative to the trap are shown in Fig. 1(b). An applied magnetic field of ≈ 0.31 mT with the orientation given in Fig. 1(b) is sufficient to avoid any dark states, independent of the polarization state of any of the lasers.

Probabilities for decay from $P_{3/2}$ to $S_{1/2}$, $D_{3/2}$, and $D_{5/2}$ are here denoted p_1 , p_2 , and p_3 , respectively. They are inferred from population measurements following the optical pumping sequences shown in Fig. 2 where it is given that each sequence is preceded by preparation into the appropriate bright or dark state. Explicitly, for Fig. 2(a), any bright state population in $S_{1/2}$ is pumped with the 493-nm laser into $D_{3/2}$ and subsequent optical pumping with 585-nm light results in a population of $S_{1/2}$ and $D_{5/2}$ with probabilities p and $1 - p$, respectively. For Fig. 2(b), any bright state population in $D_{3/2}$ is pumped with the 650-nm laser into $S_{1/2}$ and subsequent optical pumping with 493-nm light results in a population of $D_{3/2}$ and $D_{5/2}$ with probabilities q and $1 - q$, respectively. For Fig. 2(c), starting from a dark state, optical pumping with 614-nm light followed by 493-nm light results in a population of $D_{3/2}$ and $D_{5/2}$ with probabilities $1 - r$ and r , respectively. The quantities p , q , and r can be readily expressed in terms of the desired p_k . Specifically,

$$p = \frac{p_1}{p_1 + p_3}, \quad q = \frac{p_2}{p_2 + p_3}, \quad (1)$$

and

$$r = \frac{p_1 p_3}{(1 - p_1)(1 - p_3)}. \quad (2)$$

*phybmd@nus.edu.sg

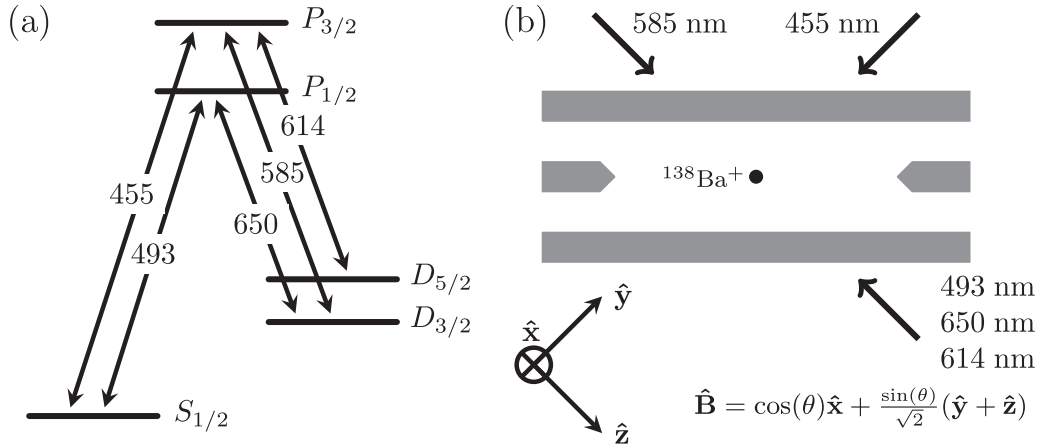


FIG. 1. (a) Level structure showing the Doppler cooling and detection transitions at 493 and 650 nm, and optical pumping transitions at 455, 585, and 614 nm. (b) Beam configurations relative to the trap. The magnetic field is specified with respect to the axes shown and has $\theta \approx 33^\circ$.

Since $\sum p_k = 1$, only two measurements are needed to uniquely determine p_k . In addition, each of the sequences in Fig. 2 can be repeated m times within a single experiment to provide measurements of p^m , q^m , and $1 - r^m$. This can provide better statistics with a similar approach having been demonstrated with Ca^+ [20]. Here we provide measurements of p and q , and use measurements of p^m and $1 - r^m$ over a range of m to check for consistency.

III. MEASUREMENTS

A. Measurement of q

Measurements of q involved optical pumping with lasers at 650, 455, and 614 nm with measured pumping time constants of 0.3, 1.0, and 1.3 μs , respectively. However, as the 455-nm laser was only locked by a wavemeter, occasional frequency excursions of ≈ 10 MHz could occur, significantly changing the pumping rate. Consequently, the pump rate was also measured within each cycle of the experiment. In addition, measurements of a dark and bright state were also made to assess the detection efficiency in each case. Thus, a single experiment cycle consisted of four interleaved experiments.

Explicit pulse sequences for each of the four experiments are given in Table I. The cooling pulse in all four cases had a duration of 400 μs and included repump light at 614 nm to ensure the atom is pumped to the bright state. The first two experiments use lasers at 455 and 650 nm to optically

pump to $D_{5/2}$; partial pumping with a 1- μs pulse monitors the pumping rate of the 455-nm transition, and complete pumping with a 30- μs pulse prepares the ion in the dark state. The third experiment uses complete optical pumping of the 455-nm transition alone to determine q , and the final experiment provides a measurement of the bright state. The full cycle was repeated in blocks of 1000. Between each block, ten measurements of the counts in 1 ms were made for both the bright state and background, where the latter was taken with the 493-nm laser turned off.

Over the course of two days, $\approx 16\,300$ blocks of data were taken. The data are conditioned on the “bright detection” from experiment 4, which gives a mean probability of 4.8×10^{-5} for detecting dark. These events are not, however, Poisson distributed. In all cases where two or more dark events occurred, they were clustered in consecutive experiments suggesting a collision event had inhibited bright detection through multiple 400- μs cooling cycles. Consequently any blocks of 1000 cycles that have more than one dark state detection event during experiment 4 were omitted. This eliminates only 15 blocks, or $\approx 0.1\%$ of the data.

From the remaining data we obtain an estimate $q = 0.108\,527(77)$, where the uncertainty is the statistical error due to projection noise. Blocks of data were also combined to give data sets of variable size N and mean values of q determined for each set to check that the data are indeed statistically limited. Values of q estimated from data sets of

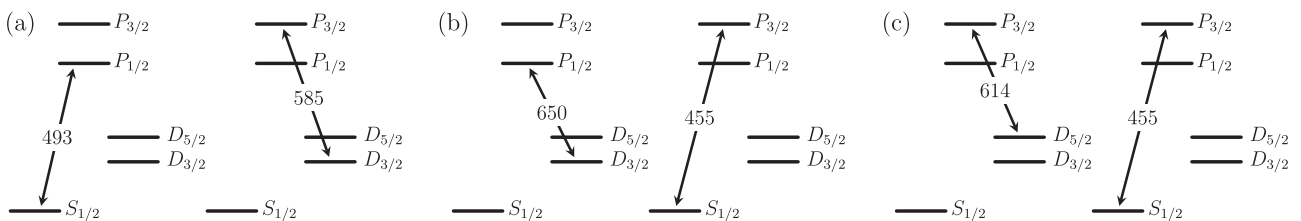


FIG. 2. Optical pumping schemes used in this paper. (a), (b), and (c) provide measurements of p , q , and $1 - r$, respectively, with p , q , r as defined in the text. Population is given to be distributed in $S_{1/2}$ and $D_{3/2}$ at the start for (a) and (b), and optically pumped to $D_{5/2}$ for (c). In each case the two steps given can be repeated with m repetitions giving populations p^m , q^m , and $1 - r^m$ in the bright states $S_{1/2}$ and $D_{3/2}$.

TABLE I. Interleaved experiments made when measuring q and the pulse sequences used for each. Cooling pulses had a duration of 400 μs and included repump light at 614 nm in addition to the detection light at 493 and 650 nm.

Expt. 1	Expt. 2	Expt. 3	Expt. 4
Cooling 650 (20 μs) 650/455 (1 μs)	Cooling 650 (20 μs) 650/455 (30 μs)	Cooling 650 (20 μs) 455 (30 μs)	Cooling
Detect.	Detect.	Detect.	Detect.

size 10^6 are given in Fig. 3(a) where the uncertainties for each point are the expected projection noise, and the associated reduced χ^2 is 0.84. The fractional standard deviation of mean values estimated from data sets of variable size N is given in Fig. 4(b) to further demonstrate that the measurement continues to average down in accordance with the projection noise limit, which is given by the solid line.

B. Measurement of p

As illustrated in Fig. 2(a), measurement of p entails optical pumping with lasers at 493 and 585 nm, which had measured pumping time constants of approximately 500 and 300 ns, respectively. The 585-nm light was generated by an 1170-nm diode laser that was locked to a frequency comb [21] and frequency doubled by a fiber-coupled, waveguide doubler. The result was a very stable scattering rate compared to that with the 455-nm laser used in the measurement of q . Thus, the typical experiment cycle consisted of only two interleaved experiments: a bright state detection, to monitor collision events, and the measurement of p . The latter consisted of 400 μs of Doppler cooling, 40 μs of optical pumping of the 493-nm transition to $D_{3/2}$, 40 μs of optical pumping with

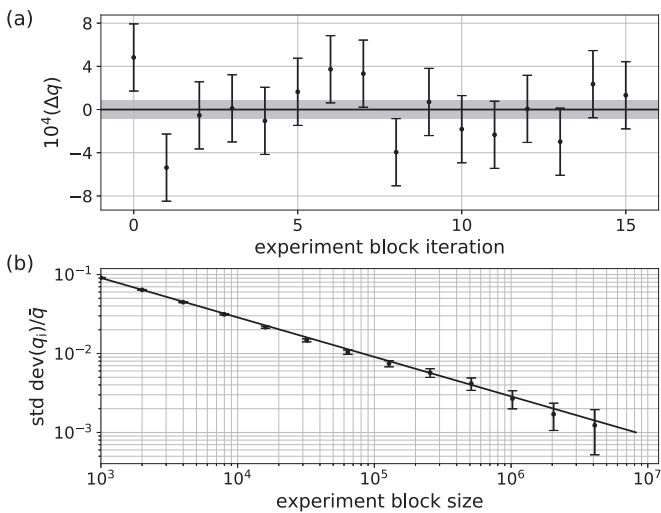


FIG. 3. Results for the measurements of q . (a) Mean values of q estimated from data sets of size $N = 10^6$, with Δq denoting the value relative to the mean of all data. Uncertainties for each point are the expected projection noise for the given N , and the shaded region is the uncertainty in the mean of all data. (b) Fractional standard deviation of mean values estimated from sets of size N .

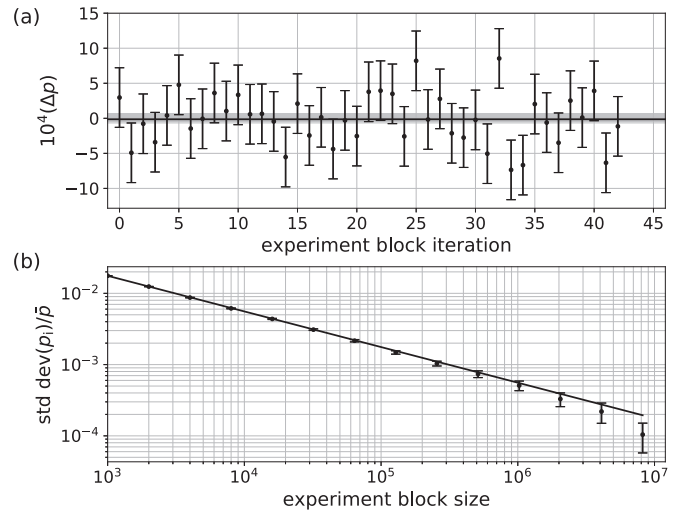


FIG. 4. Results for the measurements of p . (a) Mean values of p estimated from data sets of size $N = 10^6$, with Δp denoting the value relative to the mean of all data. Uncertainties for each point are the expected projection noise for the given N , and the shaded region is the uncertainty in the mean of all data. (b) Fractional standard deviation of mean values estimated from data sets of size N .

585-nm light, and then detection. The pumping rate of the 585-nm transition was additionally monitored in between each block to confirm its stability.

As for the measurement of q , data are conditioned on the bright state detection experiment removing 16 out of 43 100 blocks. From the remaining $\approx 43 \times 10^6$ experiments, we obtain the estimate $p = 0.763\,107(65)$. As done for q , blocks of data were combined into sets of larger size. Mean values of p estimated from datasets of size 10^6 are given in Fig. 4(a) where the uncertainties are the expected projection noise, and the associated reduced χ^2 is 0.76. The fractional standard deviation of mean values estimated from data sets of variable size N is given in Fig. 4(b) to further demonstrate that the measurement continues to average down in accordance with the projection noise limit given by the solid line.

C. Measurements of p^m and $1 - r^m$

In a similar manner to the previous two subsections, consistency checks were carried out by cycling the pumping schemes in Figs. 2(a) and 2(c) to measure p^m and $1 - r^m$ for a range of m . Values for the estimated p and r for each value of m are plotted in Fig. 5 where each measurement consists of approximately 10^6 experiments. Taking the weighted average over m in each case gives $p = 0.763\,07(11)$ and $r = 0.858\,99(10)$, where we have excluded the $m = 1$ result in the estimate for p .

The value for p is in good agreement with the $m = 1$ result $p = 0.763\,107(65)$ given in the previous section. The value of r is also in good agreement with $r = 0.859\,01(10)$ obtained from the expression

$$r = \frac{p(1-q)^2}{p+q-2pq}, \quad (3)$$

and the measured values of p and q from the previous sections.

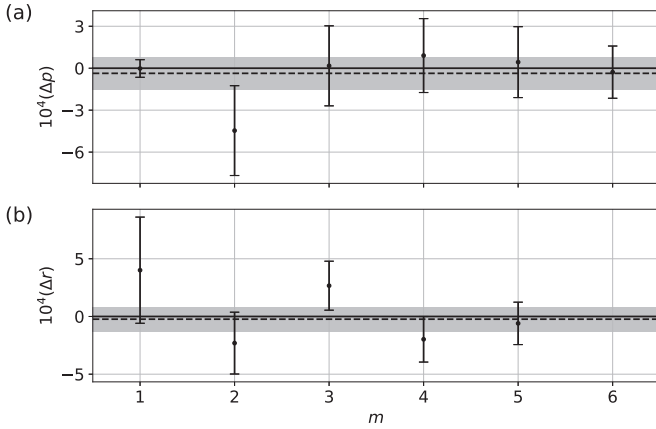


FIG. 5. Estimated values of p and r from measurements of p^m and $1 - r^m$ where m is the number of pumping cycles within a single experiment as discussed in the text. Values for p are relative to the $m = 1$ result found in Sec. III B. Values for r are given relative to the value found using Eq. (4) and values of p and q from Secs. III A and III B. In both cases, the dashed line is the weighted mean over m and the shaded region is the corresponding uncertainty. The weighted mean for p excludes the $m = 1$ result.

D. $D_{5/2}$ lifetime

A recent measurement [22] gave a $D_{5/2}$ lifetime of 25.6(0.5) s, which was significantly less than previous experimental reports [23–27] and numerous calculations [28]. As it factors into consideration of systematic effects, we provide our own measurement for reference purposes. Our method continuously monitored a string of four ions initialized with typically one or two ions in the bright state and registered when each ion became bright. Detection light was imaged onto an electron multiplying charged-coupled device camera with an imaging system having sufficient resolution to resolve the state of individual ions from a 10-ms exposure with typically better than 99% efficiency. Images were captured every 20 ms until all ions were detected bright, which was verified by a further ten images. In these experiments, the 614-nm light was physically blocked by a beam block at all times.

The initial state of the ion string was set by optical pumping to $|S_{1/2}, m = 1/2\rangle$ and driving $|S_{1/2}, m = 1/2\rangle \leftrightarrow |D_{5/2}, m = 1/2\rangle$ with a clock laser at 1762 nm. Ideally, the initial string would have one bright ion to facilitate sympathetic cooling for other ions in $D_{5/2}$. However, the configuration could only be done probabilistically, which depends on the spatial profile of the beam, and pulse duration of the clock laser. Instances in which no ions are transferred to $D_{5/2}$ simply trigger a restart. Records starting with all ions dark are still used, so long as ions appear bright one at a time and the crystal is stable. An example of ion number and configuration extracted from a given record is shown in Fig. 6(a).

Within the detection records, there are four identifiable events in addition to the expected transition to the bright state: detection errors, swaps, melts, and dark transitions. Detection errors are identified by a single image that is different from previous and subsequent images. Swaps, as the name would imply, are a change in the ion configuration without a change

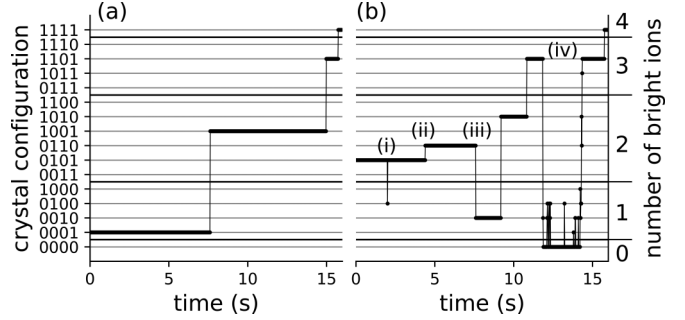


FIG. 6. (a) A typical record of an ion string monitored over time as ions in $D_{5/2}$ decay to a bright state. The binary string on the left vertical axis denotes the ion configuration with 1 representing bright and 0 dark. (b) The types of errors that can be accounted for: (i) detection error, (ii) swap, (iii) dark transition, and (iv) a melt where it recrystallizes with the same number of bright ions. The data in (b) are not an actual data record but reconstructed from multiple records for the purposes of illustration.

in number of bright ions. Melts are characterized by all ions appearing dark for several images. They are presumably the result of a high impact collision, which destabilizes the ion crystal and may take several seconds to recrystallize. Finally, dark transitions are identified by a decrease in the number of bright ions and are the result of very rare, off-resonant excitation of the 493-nm cooling light. Examples of each are shown in Fig. 6(b), which has been constructed from multiple data sets for illustration purposes.

Approximately 32 h of data were collected from the same string of four ions with a total 2429 detection records starting with at least one dark ion. An additional 48 records were discarded as quantum jumps could not be unambiguously identified due to (a) multiple ions appearing bright when starting from an all dark state (9 records); (b) the all bright verification step failing, indicating that a detection error triggered the last event (25 records); (c) the number of bright ions changing after a melting event (11 records); or (d) multiple ions transitioning at the same time (3 records).

Within the 2429 detection records there were 5620 bright transitions, 179 detection errors, 253 swaps, 50 melts, and 20 dark transitions. As all quantum jumps are recorded, the average of all bright transition times, $\tau_D = 30.14(40)$ s, is the unbiased estimate of the lifetime. In Fig. 7, we give a histogram of all recorded bright transition times in 5-s bins. The final bin is the total of all events over 100 s. Black dots and the uncertainties are theoretical expectations given the estimated τ_D and number of events recorded. The reduced χ^2 for the observed histogram is 0.99.

Note that it is important that all quantum jumps are observed in a given record when using this approach. When monitoring the decay of N ions, the time for the first decay is governed by an exponential distribution with parameter $N\lambda$, where λ is the decay rate for one ion. Hence, an observed set of times $\{T_k\}$ has a distribution

$$\begin{aligned}
 P(\{T_k\}) &= e^{-N\lambda T_1} e^{-(N-1)\lambda(T_2-T_1)} \dots e^{-\lambda(T_N-T_{N-1})} \\
 &= \prod_k e^{-\lambda T_k},
 \end{aligned} \tag{4}$$

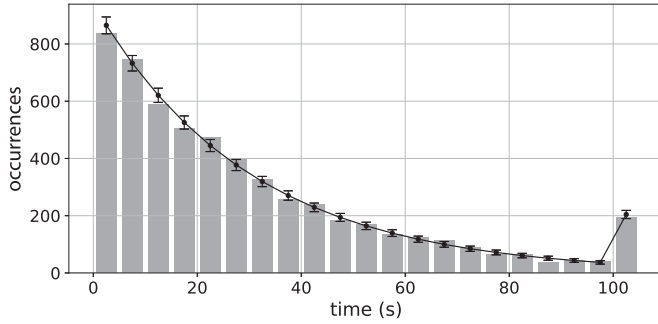


FIG. 7. Histogram of observed decay times from $D_{5/2}$. Black dots are the expected values from the estimated $\tau_D = 30.14(40)$ and number of events recorded, with the uncertainty indicating the expected standard deviation. The reduced χ^2 for the observed histogram is 0.99.

which is the expected N independent, identical distributions for a single decay. This would not be the case if some events were missed.

With the exception of the most recent report [22], the value of τ_D is consistent with previous reports [23–27] and a number of theoretical estimates [28]. Collision-induced decays are not likely significant in this experiment; of the 5620 observed decays, only 12 included an observable change in the ion configuration. In any case, such effects would decrease the observed lifetime. It may be argued that records starting with all ions dark may bias the result with possibly hotter ions requiring more time to be detectable. However, omitting all such records from the analysis yields a lifetime of 29.91(45) s, which is in good agreement with the quoted value. Moreover, if this were not the case, the histogram in Fig. 7 would not be consistent with a simple decay.

IV. SYSTEMATICS

The experiments only involve optical pumping and state detection, which results in relatively few considerations for systematic effects. These are finite optical pumping times, unwanted scattering from leakage light, finite lifetime of $D_{3/2}$ and $D_{5/2}$, collisions, and detection errors. The effect of finite lifetimes for $D_{3/2}$ and $D_{5/2}$ has the same effect as leakage light at 650 and 614 nm, respectively, and is considered in this context. Similarly collisions and detection errors are also considered in a similar context.

A. Finite pumping times

With the exception of the lasers at 455 and 614 nm, which were locked to a wavemeter, all others lasers were locked to stable references giving correspondingly stable pumping rates. In the latter cases pumping times were more than 20 time constants of the associated pumping rates, corresponding to a probability of $< 2 \times 10^{-9}$ for pumping errors. Hence only the 455- and 614-nm pumping times might be of concern.

As noted in Sec. III B, the 455-nm pumping rate was monitored in an interleaved experiment during the measurement of p by measuring the population after partial pumping for a fixed time. From these measurements the pumping rate was estimated and a histogram of the associated time

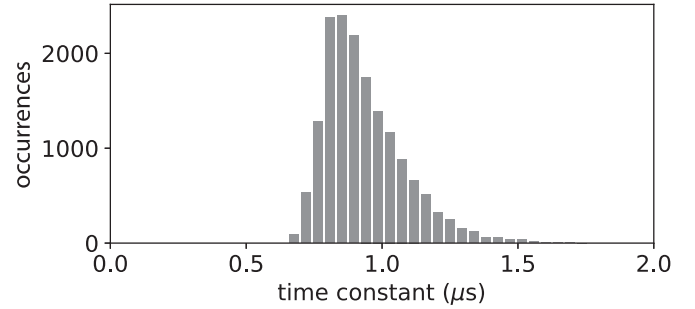


FIG. 8. Histogram of the estimated time constants associated with the 455-nm pumping rate determined throughout the measurement of p . These can be compared to the total pumping time of 40 μ s used in the experiment.

constant is given in Fig. 8. Almost all experiment cycles have pumping times more than 20 time constants of the measured pumping rates, rendering this effect negligible at the $\lesssim 10^{-8}$ level. Repumping on the 614-nm transition occurs during the 400- μ s cooling which is far longer than the pumping time constant and thus insensitive to variations. The pumping rates for transitions at 455 and 614 nm were not monitored during the measurements of p^m and $1 - r^m$ in Sec. III C. However, the consistency of those results with the independently measured p and q demonstrates that the finite pumping times are not important to the accuracy reported.

B. Leakage pumping rates

Here we describe the effects of stray light from each of the lasers and the experiments used to bound their effects. If a laser was not needed for any measurements in Sec. III, it is given that it was physically blocked and not merely switched off via an acousto-optic modulator (AOM).

1. Stray light at 455 nm

The 455-nm laser was derived from a 910-nm diode laser, which was switched by a double-pass AOM before a single-pass frequency doubling crystal. Hence the extinction ratio was very high. This was tested by optical pumping into $S_{1/2}$, and waiting 10 ms before detection and cooling (with light at 614 nm blocked). In ≈ 672 -k cycles we observed one event pumping to $D_{5/2}$ with three others attributed to collisions. The latter are identified by a sudden drop in counts that slowly recovers to the normal level.

The main effect of stray light at 455 nm would be to influence bright state detection, by pumping into the dark state, and measurements made of r^m , by repumping during pumping of the 614-nm transition. In any case, given a pumping rate of $\lesssim 1 \text{ h}^{-1}$ and the typical experiment time of $< 400 \mu$ s including pumping and detection, the probability of unwanted pumping is $\lesssim 1 \times 10^{-7}$.

2. Stray light at 614 nm

Stray light from the 614-nm laser effectively decreases the lifetime of the $D_{5/2}$ level, which was measured to be 30.14(40) s on a four ion string, as described in Sec. III D. To test the leakage rate, we repeated this lifetime measurement

with the 614-nm light unblocked but the switching AOM off. A neutral density filter attenuating the 614-nm beam was removed to give maximum pumping rate with the AOM on, which was measured to be ≈ 420 ns at the time of this test. From 239 decay events, we get an estimated lifetime of 29.7(1.9) s. This implies a scattering rate of $0.7 \pm 2.2 \times 10^{-3} \text{ s}^{-1}$ consistent with zero. Taking $3 \times 10^{-3} \text{ s}^{-1}$ as an estimated upper bound, the probability of scattering during the experiment is $\lesssim 1 \times 10^{-6}$. During the actual data runs the measured pumping time constant was $\approx 1 \mu\text{s}$ so the leakage scattering rate likewise would be smaller.

3. Stray light at 585 nm

Similar to the 455-nm laser, the switch AOM for the 585-nm beam was placed before the doubling stage, resulting in high extinction. As an initial test, the ion was left continuously scattering with the 585-nm light “off,” but unblocked, for about 0.5 h with no dark events. A further test was done by pumping to $D_{3/2}$ and waiting for 10 ms before detection and cooling (with light at 614 nm blocked). In 480 000 experiments, we observed only one pumping event and two collisions. As with stray light at 455 nm, given a pumping rate of $\lesssim 10^{-3} \text{ s}^{-1}$ and typical experiment time of $< 400 \mu\text{s}$ including pumping and detection, the probability of unwanted pumping is then $\lesssim 4 \times 10^{-7}$.

4. Stray light at 650 nm

Stray light from the 650-nm laser effectively decreases the lifetime of $D_{3/2}$. Unlike light at 455, 614, and 585 nm, stray light at 650 nm does not affect results at the detection step and thus one is only concerned with scattering during the pumping steps. A test for any leakage light at 650 nm was done by pumping to $D_{3/2}$ and waiting for $\tau_w = 20$ ms with light at 455 nm on before detection and cooling. If a scattering event on the 650-nm transition results in a decay into $S_{1/2}$, it is then pumped to $D_{5/2}$ by light at 455 nm with probability $(1 - q) \sim 0.9$.

From 872 000 cycles, we measured a dark probability of $p_d = 2.85(18) \times 10^{-3}$. From the 79.8(4.6)-s lifetime of $D_{3/2}$, we would expect a $2.5(3) \times 10^{-4}$ probability of decay to $S_{1/2}$ in 20 ms, of which $1 - q$ will be pumped dark by light at 455 nm. The observed rate is thus dominated by scattering on the 650-nm transition, and the rate of scattering out of $D_{3/2}$ is $\gamma_s = p_d / [\tau_w(1 - q)] = 0.15 \text{ s}^{-1}$. This effectively reduces the lifetime of $D_{3/2}$ to about 6.5 s.

For measurements of p , there is little opportunity for leakage light at 650 nm to cause a problem because light at 585 nm will depopulate $D_{3/2}$ on a timescale of $1 \mu\text{s}$. So the error caused by leakage light at 650 nm can only be $\approx 1 \times 10^{-7}$. During measurements of q , decay of the population from $D_{3/2}$ during the $30 \mu\text{s}$ of optical pumping on the 455-nm transition will be more significant. Since the 455-nm optical pumping rate is much shorter than the pumping time, we make the approximation that any $D_{3/2}$ decay is immediately pumped to $D_{5/2}$ with probability $1 - q$. The error is then $\gamma_s \times 30 \mu\text{s} \times (1 - q) \approx 4 \times 10^{-6}$.

5. Stray light at 493 nm

The 493-nm beam is double passed by two AOMs and the measured extinction was in excess of 130 dB. We nonetheless attempted to measure this by pumping to $S_{1/2}$, waiting 10 ms before optical pumping on the 585-nm transition before detection and cooling, all with light at 614 nm blocked. From 40 000 cycles we saw no shelving events. Thus the scattering rate out of $S_{1/2}$ would be $\lesssim 10^{-3} \text{ s}^{-1}$. As with stray light at 650 nm, this does not affect detection, and hence the error is $\lesssim 4 \times 10^{-8}$.

C. Collisions and detection errors

For the experiments reported here, the dominant effect of collisions would be to interrupt detection by disrupting fluorescence for an ion in a bright state. As noted in Sec. III, collision events that disrupt multiple experiments are readily identified in the data and removed. However, events that influence a single experiment cannot be readily identified. Nevertheless we would still expect such an event to result in a bright state detection error, and consequently this rate can bound the influence of collisions on the measurement. Indeed one might even argue that the bright state detection efficiency would be ultimately limited by such collisions.

For the branching ratio measurements reported here we used a Bayesian detection scheme [29,30] in which the bright (dark) state probability is estimated in real time and terminates when the bright (or dark) state probability falls below a preset threshold, here set to 10^{-6} . Count rates during the experiments were typically in the range $\approx 35\text{--}40$ counts/ms for a bright state, and a more stable 0.4 counts/ms for a dark state.

From the measurements sequences used for q , the observed probability of detecting dark during experiment 4 was $\epsilon_b = 7.2(7) \times 10^{-6}$, which is taken as an estimate of a bright state detection error. Similarly, the probability of detecting a bright state during experiment 2 was $\epsilon_d = 1.9(1) \times 10^{-5}$, which is taken as an estimate of a dark state detection error. In both cases the observed error rates are significantly above the 10^{-6} thresholds set in the Bayesian detection algorithm. Possible causes for excess detection errors would be collisions and the $D_{5/2}$ lifetime for bright and dark states, respectively.

The bright state control experiments taken during the measurements of p and q and records for the $D_{5/2}$ lifetime measurement gave clear evidence of collisions. From the collision events identified in the measurements of p and q , the estimated collision rate would be roughly 1 every 48 min. Similarly data from the $D_{5/2}$ lifetime suggest a collision rate of 1 every 6 min, which is roughly consistent given the larger number of ions. Collision events occurring on this timescale, however, would not significantly contribute to the observed error rates, as these events were detected and removed. However, those events were collisions with sufficient impact to interrupt cooling over many experimental cycles. Less impactful collisions that interrupt only a single experiment would likely have a higher rate. We also note that varying fluorescent rates can influence the validity of the threshold. Simulations and independent experiments indicate this can be as much as a factor of 4 for a 10% drop in fluorescence. In any case, the observed bright state error rate is not significant at the level of the statistical uncertainties in the reported results.

TABLE II. Probabilities for decay from $P_{3/2}$ to $S_{1/2}$, $D_{3/2}$, and $D_{5/2}$, which are denoted p_1 , p_2 , and p_3 , respectively. Values are determined from the measured values of p and q given in Eq. (7). Theory values were estimated as discussed in [17].

	p_1	p_2	p_3
Expt.	0.741717(71)	0.028031(23)	0.230253(62)
Theory	0.7423(18)	0.0280(2)	0.2297(15)

For the dark state control experiment, decay during detection would likely trigger a bright state result. The probability of this occurring depends on the distribution of detection times. For our detection parameters, the average time to detect a dark state is $\approx 400 \mu\text{s}$ and the expected probability to decay within this time is 1.3×10^{-5} . Although clearly a contributing factor, it is still smaller than the observed error rate. This could be due to state preparation errors associated with pumping into the dark state.

Whatever the source of detection errors, the resulting measured probability p_m of a true probability p would be given by

$$p_m = p(1 - \epsilon_b) + (1 - p)\epsilon_d = p + [(1 - p)\epsilon_d - p\epsilon_b]. \quad (5)$$

The term in square brackets is then a systematic shift. For the observed error rates ϵ_b and ϵ_d , this would be at most 20% of the statistical error for the determination of q , and hence we neglect it.

V. DISCUSSION

The dominant systematics in the branching ratios reported here are from detection errors and are not significant at the level of the statistical uncertainties. Thus our final values are given by

$$p = 0.763107(65) \quad \text{and} \quad q = 0.108527(77). \quad (6)$$

From these we can calculate the probabilities for decay from $P_{3/2}$ to $S_{1/2}$, $D_{3/2}$, and $D_{5/2}$, denoted p_1 , p_2 , and p_3 , respectively. Values are given in Table II along with those calculated from theory for comparison. As discussed in [17], theory values were calculated using a linearized coupled-cluster approach including single-double excitations with uncertainties estimated from additional calculation methods.

The experimental values of p_k differ by two to three standard deviations of the results reported in [8], but are in reasonable agreement with the values predicted in our previous work [17]. The latter used measured branching fractions for decays from $P_{1/2}$, experimental matrix elements from [4], and theoretical estimates of matrix element ratios. With the above branching fractions and the reduced matrix element $\langle P_{3/2} \| r \| S_{1/2} \rangle = 4.7017(27)$ a.u. reported in [4], matrix elements associated with $P_{3/2}$ decays and the lifetime can now be obtained using only experimentally determined values. The remaining matrix elements are found to be

$$\langle P_{3/2} \| r \| D_{5/2} \rangle = 4.1028(25) \text{ a.u.}, \quad (7a)$$

$$\langle P_{3/2} \| r \| D_{3/2} \rangle = 1.33199(96) \text{ a.u.}, \quad (7b)$$

TABLE III. Matrix elements ratios R_0 , R_2/R_1 , R_1/R_0 , and R_2/R_0 , where R_k are as given in Eq. (8). Experimental values are derived from the measured values of p and q given in Eq. (7), matrix elements reported in [4], and the $P_{1/2}$ branching fraction reported in [17]. Theory values were estimated as discussed in [17].

	Expt.	Theory
R_0	1.4140(17)	1.4109(2)
R_2/R_1	0.32466(13)	0.32473(32)
R_1/R_0	0.95406(22)	0.95338(38)
R_2/R_0	0.30974(14)	0.30959(18)

which yield a lifetime of $\tau(P_{3/2}) = 6.2615(72)$ ns or linewidth $\Gamma = 2\pi \times 25.418(29)$ MHz. For all quantities, uncertainties are taken as the usual 1σ and added in quadrature with the dominant contribution being from the reduced matrix element, $\langle P_{3/2} \| r \| S_{1/2} \rangle$.

The matrix elements given in Eq. (7) are in excellent agreement with theoretical calculations [16], but differ from estimates obtained using experimental results combined with ratios of matrix elements calculated from theory [17]. The ratios in question are

$$R_0 = \frac{\langle 6P_{3/2} \| r \| 5S_{1/2} \rangle}{\langle 6P_{1/2} \| r \| 5S_{1/2} \rangle}, \quad (8a)$$

$$R_1 = \frac{\langle 6P_{3/2} \| r \| 5D_{5/2} \rangle}{\langle 6P_{1/2} \| r \| 5D_{3/2} \rangle}, \quad (8b)$$

and

$$R_2 = \frac{\langle 6P_{3/2} \| r \| 5D_{3/2} \rangle}{\langle 6P_{1/2} \| r \| 5D_{3/2} \rangle}, \quad (8c)$$

which can now be obtained from the experimental results in [4], the $P_{1/2}$ branching ratio reported in [17], and values given in Eq. (7). Specifically we have

$$R_1 = \sqrt{\left(\frac{1-p}{p}\right)\left(\frac{1-\bar{p}}{\bar{p}}\right)} \left(\frac{\omega_{455}\omega_{650}}{\omega_{614}\omega_{493}}\right)^{3/2} R_0 \quad (9)$$

and

$$R_2 = \sqrt{\frac{q}{1-q}} \left(\frac{\omega_{614}}{\omega_{585}}\right)^{3/2} R_1, \quad (10)$$

where \bar{p} is the branching fraction for the $P_{1/2}$ level reported in [17].

Values for R_0 , R_2/R_1 , R_1/R_0 , and R_2/R_0 obtained from experimental results are given in Table III. Uncertainties are derived in the usual manner by taking the quadrature sum of independent contributions with the exception of R_0 for which relative uncertainties from each matrix element are added to allow for possible correlation in their determination. Theory values are also given for comparison with uncertainties determined from the maximum discrepancy between different computation methods [17]. As noted in [17], calculated ratios are expected to be accurate as they depend only weakly on correlation corrections. Consequently, the 1.8σ and 1.6σ in the difference for R_0 and R_1/R_0 between experiment and theory may be significant. We would therefore recommend a 2σ estimate of uncertainties for derived quantities such as the

matrix elements in Eq. (7) and the corresponding estimates of τ and Γ .

In general, theoretical calculations for Ba^+ are in excellent agreement with experimental results derived from the matrix elements reported in [4] and branching ratios reported here and in [17]. In all cases the matrix elements are better than 1% of the experimentally determined values. As branching fractions provide ratios of matrix elements, all values are tied to the values of $\langle P_{3/2} || r || S_{1/2} \rangle$ and $\langle P_{1/2} || r || S_{1/2} \rangle$ reported in [4]. Thus, it would be of interest to confirm those results by a different methodology such as that demonstrated in [31,32]. However, it would likely be difficult to reach a comparable level of accuracy via that approach.

In summary we have provided branching ratio measurements for decays from $P_{3/2}$. The values are more than an order of magnitude more accurate than those given in previous reports and measurements have been done in two different ways to check for consistency. Together with results in [4,17],

they provide a complete set of experimentally determined matrix elements for all the dominant contributions to the differential scalar polarizability, $\Delta\alpha_0(\omega)$ of the $S_{1/2} \leftrightarrow D_{5/2}$ clock transition. In addition, we have provided a measurement of the $D_{5/2}$ lifetime, which also improves upon previous values.

ACKNOWLEDGMENTS

This work is supported by the National Research Foundation, Prime Ministers Office, Singapore and by the Ministry of Education, Singapore under the Research Centres of Excellence program. It is also supported by the National Research Foundation, Singapore, hosted by National University of Singapore under its Quantum Engineering Program (Grant No. QEP-P5). M.S.S. acknowledges the sponsorship of the Office of Naval Research, Grant No. N00014-17-1-2252.

-
- [1] G. Marx, G. Tommaseo, and G. Werth, Precise g_J - and g_I -factor measurements of Ba^+ isotopes, *Eur. Phys. J. D* **4**, 279 (1998).
- [2] K. H. Knöll, G. Marx, K. Hübner, F. Schweikert, S. Stahl, Ch. Weber, and G. Werth, Experimental g_J factor in the metastable $5D_{3/2}$ level of Ba^+ , *Phys. Rev. A* **54**, 1199 (1996).
- [3] M. R. Hoffman, T. W. Noel, C. Auchter, A. Jayakumar, S. R. Williams, B. B. Blinov, and E. N. Fortson, Radio-frequency-spectroscopy measurement of the Landé g_J factor of the $5D_{5/2}$ state of Ba^+ with a single trapped ion, *Phys. Rev. A* **88**, 025401 (2013).
- [4] S. L. Woods, M. E. Hanni, S. R. Lundeen, and E. L. Snow, Dipole transition strengths in Ba^+ from Rydberg fine-structure measurements in Ba and Ba^+ , *Phys. Rev. A* **82**, 012506 (2010).
- [5] J. A. Sherman, A. Andalkar, W. Nagourney, and E. N. Fortson, Measurement of light shifts at two off-resonant wavelengths in a single trapped Ba^+ ion and the determination of atomic dipole matrix elements, *Phys. Rev. A* **78**, 052514 (2008).
- [6] N. Kurz, M. R. Dietrich, G. Shu, R. Bowler, J. Salacka, V. Mirgon, and B. B. Blinov, Measurement of the branching ratio in the $6P_{3/2}$ decay of Ba II with a single trapped ion, *Phys. Rev. A* **77**, 060501(R) (2008).
- [7] D. De Munshi, T. Dutta, R. Rebhi, and M. Mukherjee, Precision measurement of branching fractions of $^{138}\text{Ba}^+$: Testing many-body theories below the 1% level, *Phys. Rev. A* **91**, 040501(R) (2015).
- [8] T. Dutta, D. De Munshi, D. Yum, R. Rebhi, and M. Mukherjee, An exacting transition probability measurement—a direct test of atomic many-body theories, *Sci. Rep.* **6**, 29772 (2016).
- [9] C. Guet and W. R. Johnson, Relativistic many-body calculations of transition rates for Ca^+ , Sr^+ , and Ba^+ , *Phys. Rev. A* **44**, 1531 (1991).
- [10] V. A. Dzuba, V. V. Flambaum, and J. S. M. Ginges, Calculations of parity-nonconserving $s-d$ amplitudes in Cs, Fr, Ba^+ , and Ra^+ , *Phys. Rev. A* **63**, 062101 (2001).
- [11] E. Iskrenova-Tchoukova and M. S. Safronova, Theoretical study of lifetimes and polarizabilities in Ba^+ , *Phys. Rev. A* **78**, 012508 (2008).
- [12] U. I. Safronova, Relativistic many-body calculation of energies, lifetimes, hyperfine constants, multipole polarizabilities, and blackbody radiation shift in ^{137}Ba II, *Phys. Rev. A* **81**, 052506 (2010).
- [13] B. K. Sahoo, B. P. Das, R. K. Chaudhuri, and D. Mukherjee, Theoretical studies of the $6s^2S_{1/2} \rightarrow 5d^2D_{3/2}$ parity-nonconserving transition amplitude in Ba^+ and associated properties, *Phys. Rev. A* **75**, 032507 (2007).
- [14] G. Gopakumar, H. Merlitz, R. K. Chaudhuri, B. P. Das, U. S. Mahapatra, and D. Mukherjee, Electric dipole and quadrupole transition amplitudes for Ba^+ using the relativistic coupled-cluster method, *Phys. Rev. A* **66**, 032505 (2002).
- [15] N. Fortson, Possibility of Measuring Parity Nonconservation with a Single Trapped Atomic Ion, *Phys. Rev. Lett.* **70**, 2383 (1993).
- [16] M. D. Barrett, K. J. Arnold, and M. S. Safronova, Polarizability assessments of ion-based optical clocks, *Phys. Rev. A* **100**, 043418 (2019).
- [17] K. J. Arnold, S. R. Chanu, R. Kaewuam, T. R. Tan, L. Yeo, Z. Zhang, M. S. Safronova, and M. D. Barrett, Measurements of the branching ratios for $6P_{1/2}$ decays in $^{138}\text{Ba}^+$, *Phys. Rev. A* **100**, 032503 (2019).
- [18] K. J. Arnold, R. Kaewuam, A. Roy, T. R. Tan, and M. D. Barrett, Blackbody radiation shift assessment for a lutetium ion clock, *Nat. Commun.* **9**, 1650 (2018).
- [19] R. Kaewuam, A. Roy, T. R. Tan, K. J. Arnold, and M. D. Barrett, Laser spectroscopy of $^{176}\text{Lu}^+$, *J. Mod. Opt.* **65**, 592 (2018).
- [20] R. Gerritsma, G. Kirchmair, F. Zähringer, J. Benhelm, R. Blatt, and C. F. Roos, Precision measurement of the branching fractions of the $4p^2P_{3/2}$ decay of Ca II, *Eur. Phys. J. D* **50**, 13 (2008).
- [21] R. Kaewuam, T. R. Tan, K. J. Arnold, and M. D. Barrett, Spectroscopy of the $^1S_0 - ^1D_2$ clock transition in $^{176}\text{Lu}^+$, *Phys. Rev. A* **99**, 022514 (2019).
- [22] E. A. Dijck, A. Mohanty, N. Valappol, M. Nuñez Portela, L. Willmann, and K. Jungmann, Lifetime of the $5d^2D_{5/2}$ level of $^{138}\text{Ba}^+$ from quantum jumps with single and multiple $^{138}\text{Ba}^+$ ions, *Phys. Rev. A* **97**, 032508 (2018).

- [23] C. Auchter, T. W. Noel, M. R. Hoffman, S. R. Williams, and B. B. Blinov, Measurement of the branching fractions and lifetime of the $5D_{3/2}$ level of Ba^+ , *Phys. Rev. A* **90**, 060501 (2014).
- [24] J. Gurell, E. Biémont, K. Blagoev, V. Fivet, P. Lundin, S. Mannervik, L.-O. Norlin, P. Quinet, D. Rostohar, P. Royen *et al.*, Laser-probing measurements and calculations of lifetimes of the $5d\ ^2D_{3/2}$ and $5d\ ^2D_{5/2}$ metastable levels in Ba II, *Phys. Rev. A* **75**, 052506 (2007).
- [25] P. Royen, J. Gurell, P. Lundin, L.-O. Norlin, and S. Mannervik, Monitoring the weak collisional excitation of a stored ion beam reveals the radiative decay rate of extremely long-lived metastable levels, *Phys. Rev. A* **76**, 030502 (2007).
- [26] W. Nagourney, J. Sandberg, and H. Dehmelt, Shelved Optical Electron Amplifier: Observation of Quantum Jumps, *Phys. Rev. Lett.* **56**, 2797 (1986).
- [27] A. A. Madej and J. D. Sankey, Quantum jumps and the single trapped barium ion: Determination of collisional quenching rates for the $5d\ ^2D_{5/2}$ level, *Phys. Rev. A* **41**, 2621 (1990).
- [28] U. I. Safronova, M. S. Safronova, and W. R. Johnson, Forbidden M1 and E2 transitions in monovalent atoms and ions, *Phys. Rev. A* **95**, 042507 (2017), and references therein.
- [29] E. Paez, K. J. Arnold, E. Hajiyev, S. G. Porsev, V. A. Dzuba, U. I. Safronova, M. S. Safronova, and M. D. Barrett, Atomic properties of Lu^+ , *Phys. Rev. A* **93**, 042112 (2016).
- [30] A. H. Myerson, D. J. Szwerc, S. C. Webster, D. T. C. Allcock, M. J. Curtis, G. Imreh, J. A. Sherman, D. N. Stacey, A. M. Steane, and D. M. Lucas, High-Fidelity Readout of Trapped-Ion Qubits, *Phys. Rev. Lett.* **100**, 200502 (2008).
- [31] M. Hettrich, T. Ruster, H. Kaufmann, C. F. Roos, C. T. Schmiegelow, F. Schmidt-Kaler, and U. G. Poschinger, Measurement of Dipole Matrix Elements with a Single Trapped Ion, *Phys. Rev. Lett.* **115**, 143003 (2015).
- [32] K. J. Arnold, R. Kaewuam, T. R. Tan, S. G. Porsev, M. S. Safronova, and M. D. Barrett, Dynamic polarizability measurements with $^{176}Lu^+$, *Phys. Rev. A* **99**, 012510 (2019).